Bull. Mater. Sci., Vol. 40, No. 7, December 2017, pp. 1503–1511
https://doi.org/10.1007/s12034-017-1511-0

Tailoring the bandgap and magnetic properties by bismuth substitution in neodymium chromite

VENKATESWARA RAO MANNEPALLI, M M SAJ MOHAN and R RANJITH*
Department of Materials Science and Metallurgical Engineering, Indian Institute of Technology Hyderabad, Kandi, Sanga Reddy 502285, India
*Author for correspondence (ranjith@iith.ac.in)

MS received 23 December 2016; accepted 26 April 2017; published online 30 November 2017

Abstract. The intrinsic distortions present in rare-earth orthochromites ($RCrO_3$) observed from lanthanum to lutetium (in R-site) can influence the magnetic properties like Neel transition and weak ferromagnetic coupling. A nonmagnetic cation with similar ionic radius would be a suitable candidate to engineer the inherent distortions of particular orthochromite. In this study, bismuth (Bi^{3+}) with a $6s^2$ lone pair was chosen to substitute in neodymium (Nd^{3+}) site of $NdCrO_3$ (NCO) to tailor the intrinsic structural distortions. The variation of optical absorption edge evidently suggests that Bi ($6s^2$) substituted in the magnetic rare-earth Nd^{3+} influences the Cr–O overlap integral. The interaction of Bi cation with oxygen bonds influences the structural distortions through Cr–O polyhedral, which are evident from Raman scattering studies. The observed structural and magnetic properties of similar ionic radius of Bi^{3+} in Nd^{3+} reveal that intrinsic structural distortions are interrelated to enhanced weak ferromagnetic component and change in Neel and spin reorientation temperatures in our compounds. In addition, a reduction in the optical bandgap of NCO from 3.1 to 2.6 eV was observed.

Keyword. Raman spectroscopy; magnetic properties; optical bandgap.

1. Introduction

Orthochromites, $RCrO_3$ (R = rare earth), are interesting family of compounds due to intriguing physical properties and their complex magnetic interactions. These compounds have received wide attention aiming at versatile applications like solid oxide fuel cells [1,2], negative temperature coefficient (NTC) thermistors [3], multiferroic applications [4–7], etc. The intriguing ferroelectric nature of magnetic rare-earth orthochromites, $RCrO_3$ (R = Sm, Gd, Er, Tb and Tm) is expected to arise by the local symmetry breaking due to the interaction between magnetic rare-earth ion and weak ferromagnetic Cr^{3+} ions at magnetic ordering temperatures [4]. Thus, the short range polar order in chromates is due to local symmetry present in the samples [8]. In addition, the nonmagnetic nature of yttrium can also induce polar nature in $YCrO_3$ due to inherent distortions present in system [6,9,10]. On the other hand, $RCrO_3$ show extremely rich magnetic properties due to interaction between R^{3+}–R^{3+}, R^{3+}–Cr^{3+} and Cr^{3+}–Cr^{3+} ions leading to various types of magnetic ordering at different temperatures. The Cr^{3+} moments in all rare-earth orthochromite pervoskites exhibits G-type antiferromagnetic structure at Neel temperatures (T_N) ranging from 115 to 289 K and also possess weak ferromagnetic order below T_N [11–13]. Presence of magnetic moment at rare-earth site in orthochromites enhances the magnetization due to Cr^{3+} sublattice polarize R^{3+} rare-earth ions [14], which results into another transition at low temperatures called spin reorientation temperature, T_{SRPT}. Due to the interaction of R^{3+}–Cr^{3+} (R = Gd, Nd, Ho, Er, Tm) in orthochromites, the T_{SRPT} varies from 6.5 to 35 K [15–17]. The rare-earth ordering due to weak interactions among R^{3+}–R^{3+} can be observed at very low temperatures and in some compounds like $HoCrO_3$ and $PrCrO_3$, the rare-earth ordering is not at all observed within the measured temperature range [13]. Few magnetic rare-earth chromites also show magnetization reversal properties due to rare-earth moments and are aligned antiparallel to the chromium magnetic moments [15,18]. The strong among these interactions are Cr^{3+}–Cr^{3+} responsible for antiferromagnetic ordering in chromites and it is greatly influenced by the rare-earth ionic radius. A monotonic decrease of T_N is observed in series of orthochromites with decreasing of ionic radius of rare-earth and mixed orthochromites [13,14]. The observed weak ferromagnetic nature below T_N in these chromites is due to canting of the Cr^{3+} system, which arises from the Dzyaloshinsky–Moriya exchange interaction [19]. When compared, the Neel transition temperature dependence of orthoferrite with the orthochromites (isostructural and non-Jahn Teller active ions) with the variation of ionic size of rare-earth ion, the former depends on Fe^{3+}–O–Fe^{3+} bond angle [20], whereas the latter dependence on Cr^{3+}–O–Cr^{3+} bond angle is overall 30% of T_N [21]. Thus, additional intrinsic structural distortions, which lead to involvement of overlapping t and e orbitals of Cr^{+3} in orthochromites along with the bond angle dependence in chromites, can explain the observed T_N variation with ionic sizes [21]. This can be

understood from the simple picture of octahedra units built by pervoskite oxides. In a regular octahedral arrangement, when a transition metal is surrounded by six oxide ions, then $3d$ orbitals of Cr ($3d^3$) splits into two groups, a lower triplet, t_{2g} or t and an upper doublet e_g or e. The physical basis for this splitting is simply the electrostatic repulsion between the d electrons and the surrounding negative oxygen ions, where the e_g orbitals point directly at these ions and the t_{2g} orbitals point in between the ions. Although this simple picture does not take covalent bonding into account; its inclusion does not affect the fundamental result [22]. After involving the covalent bonding, it leads to exactly same kind of splitting into a lower non-bonding t_{2g} orbital and an upper antibonding e_g orbital with difference in magnitude of the energy separation between the two orbitals. Thus, the inclusion of mixed ionic and covalent character of metal to oxygen bonding in metal ion influences the T_N. However, in chromites, size or ionic radius of rare-earth cations (Lu–La) plays important roles on the structural distortions of $RCrO_3$, which makes the octahedra to be linked in canting position with each other [21,23]. These structural distortions indeed involve the change in bond angles, which further leads to inherent bond overlap of t_{2g} (filled) and e_g (unfilled) orbitals of chromium with oxygen and observed changes in T_N. Thus $t_{2g}-e_g$ hybridization is inevitable with the change of bond angle in chromites, whereas this hybridization on $Fe^{3+}(t^3e^2)$ (i.e., t^3-O-t^3 and e^2-O-e^2) did not bring any change in T_N of orthoferrites. The observed weak ferromagnetic coupling in these chromates (Cr^{3+} : t^3e^0) can be understood by the super exchange interaction between two adjacent transition metal ions is delivered by a virtual charge transfer [21] i.e., $t_{2g}^3-O-e_g^0$. Thus, understanding on orthorhombic pervoskites that possess intrinsic structural distortions in addition to the cooperative octahedral-site BO_6 (B = Fe, Cr, Mn) rotations are essential elements to interpret magnetic properties in these systems [24]. In this study, we attempt to tune the inherent structural distortions which can in turn affect the magnetic properties of $RCrO_3$, especially $NdCrO_3$. Structural [25], magnetic susceptibility [26], neutron studies [12,27] and specific heat properties [28] investigations performed on $NdCrO_3$ and also limited number of studies, such as $Nd_{1-x}Eu_xCrO_3$ [16], $Nd_{1-x}La_xCrO_3$ [29], $Nd_{1-x}Sr_xCrO_3$ [27] to understand the altered interactions among Nd and Cr in $NdCrO_3$. These studies reveal that the effect of substitution of higher ionic radius or magnetic rare-earth ions in Nd-site either dilutes the Nd–Cr coupling or decrease in the structural distortions due to increase in bond angle, further leads to increase in T_N. To understand the inherent structural distortions and its relation to magnetic properties, a nonmagnetic and similar radius of Nd^{3+} is suitable candidate for the study. At present, we have chosen an element other than rare earth, nonmagnetic bismuth cation ($r_{Bi3+} = 1.11$Å), which is prone to introduce local structural distortion due to the presence of stereo-chemically active $6s^2$ lone pair electron [30] and profoundly influence the magnetic properties. Unlike the electron configuration of Nd^{3+} ($r_{Nd3+} = 1.109$ Å) ions ($4f^3$), the outermost shell of Bi^{3+} ($6s^2$) is fully occupied. To the best of our knowledge, structural distortions interrelated magnetic and optical properties of Bi^{3+} in Nd^{3+} of $NdCrO_3$ were not reported due to high pressure synthesis [31] required for Bi-based chromates. The substitution of Bi^{3+} in $NdCrO_3$ of its own is challenging and not many efforts were carried out in orthochromites. In this study, $Nd_{1-x}Bi_xCrO_3$ (NBiCO) with varying Bi content was successfully synthesized by sol–gel route up to 15 at% Bi substituted at Nd^{3+} site.

2. Materials and methods

$Nd_{1-x}Bi_xCrO_3$ ($x = 0, 0.05, 0.1, 0.15$ at%) (NBiCO) was synthesized by the sol–gel method using the nitrates of neodymium, bismuth and chromium. Nitrates of neodymium and bismuth are prepared from the oxides dissolved in nitric acid, whereas chromium nitrate ($Cr(NO_3)_3 \cdot 9H_2O$) is obtained from the Sigma Aldrich (99% pure). The nitrates of all cations are homogeneously mixed with simultaneous addition of citric acid (chelating agent) and ethylene glycol (gelating agent). The obtained solution was dried at 393K for 2 days and then heat-treated to evaporate the nitrates. The extracted powder was calcined at 1123K for 4 h. Calcined powders were pelletized with the addition of freshly prepared polyvinyl alcohol solution as binder and sintered at 1373 K for 10 h in closed environment, to minimize the loss of bismuth. Structural analysis was performed through X-ray powder diffraction (XRD) studies at room temperature (RT ∼ 303 K) (Panalytical X'pert Pro, CuK α radiation). Rietveld refinement was performed on the powder diffraction data by using 'fullprof' software [32]. The phonon modes of all the synthesized compounds were studied using a Laser Micro Raman spectrometer (Bruker, Senterra) with an excitation source of 532 nm at RT. Magnetic

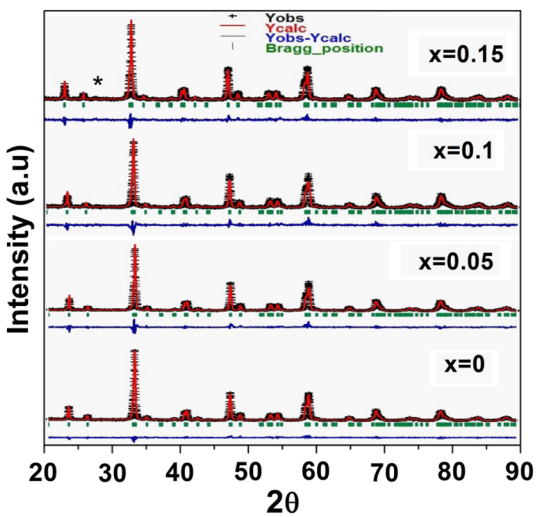

Figure 1. (colour online) XRD patterns at RT for compositions $x = 0, 0.1$ and 0.15 in $Nd_{1-x}Bi_xCrO_3$. * Indicates the minor impurity of Bi_2O_3.

measurements are carried out by Physical Property Measurement System (PPMS) Dynacool (Quantum design, USA) with magnetic fields varied from −5 to +5 T and temperature sweep from 5 to 300 K. The optical studies were done by using UV–Vis Spectrometer lambda 1050 from Perkin Elmer.

3. Results and discussion

3.1 *Structural diffraction patterns*

Rietveld refinements of NBiCO were carried out using the orthorhombic crystal system with the centrosymmetric *Pnma* space group, which shows good agreement between the observed and calculated diffraction patterns, which is shown as difference ($Y_{obs}-Y_{cal}$) plot given at the bottom ensures a reliable fit of the experimental data. The bars in figure 1 represent Bragg diffraction positions and the reasonable reliability parameters such as low R-factors and χ^2-values indicate the authencity of the refinement. The background was refined with 6th order polynomial function and pseudo-Voight is used as peak shape profile to refine the patterns. The diffraction patterns revealed that $x = 0.15$ refined with the single phase orthorhombic *Pnma* symmetry along with minor amount (<2%) of Bi_2O_3 (nonmagnetic) impurity. The observations suggest that the solubility of bismuth (Bi) in Nd site is lower than 15 at% through our sol–gel processing technique. Single phase of NBiCO and the minimal change of lattice parameters (table 1) show that the similar ionic radius of bismuth occupies the neodymium site. The observed average change in bond angles from 154 to 152° up to 10 at% through our XRD patterns. The average change in bond lengths such as Cr-O1 (1.984–1.973 Å), Nd-O1 (3.14–3.2 Å), Cr-O2 (1.97–1.95) and Nd-O2 (2.72–2.49 Å) indicates a global structure orthorhombic (*Pnma)* throughout the composition range. Even though the XRD structure remains the same, the difference of electronic configuration and sterochemical activity of 'Bi' in 'Nd' site is expected to affect the local

Table 1. Refinement details of $Nd_{1-x}Bi_xCrO_3$ ($x = 0$, 0.05 and 0.1) for orthorhombic *Pnma* space group.

Refined parameters		$x = 0$	$x = 0.05$	$x = 0.1$
a (Å)		5.4849(6)	5.4838(7)	5.4885(4)
b (Å)		7.6936(7)	7.6930(8)	7.6989(6)
c (Å)		5.4197(6)	5.4180(7)	5.4214(4)
Cr–O1		1.984(8)	1.986(9)	1.973(8)
Cr–O2		1.97(2)	1.95(3)	1.95(3)
		1.99(2)	2.01(3)	2.03(3)
Cr–O1–Cr		151.5(3)	151.1(4)	154.5(3)
Cr–O2–Cr		154.3(9)	154.2(11)	152.3(12)
Bragg R-factor (R_B)		6.54	11.6	15.5
RF-factor		5.76	9.57	13.4
χ^2		1.21	1.52	1.52
R_p		9.08	7.23	7.0
R_{wp}		11.8	9.40	9.03
R_{exp}		10.75	7.62	7.31
Thermal parameter (B) (Å^2)		1.48	2.22	2.11
Volume (Å^3)		228.7	228.6	229.1
			Positions→	
Composition	Ions↓	x	y	z
$x = 0$	Nd^{3+}/Bi^{3+}4(c)	0.0414(3)	0.25	0.0084(7)
	Cr^{3+}4(b)	0	0	0.5
	O1 4(c)	0.477(4)	0.25	−0.087(6)
	O2 8(d)	0.296(4)	0.035(4)	−0.294(4)
$x = 0.05$	Nd^{3+}/Bi^{3+}4(c)	0.0403(4)	0.25	0.0056(9)
	Cr^{3+}4(b)	0	0	0.5
	O1 4(c)	0.462(4)	0.25	−0.083(7)
	O2 8(d)	0.289(5)	0.045(4)	−0.282(5)
$x = 0.1$	Nd^{3+}/Bi^{3+}4(c)	0.0413(4)	0.25	0.0055(10)
	Cr^{3+}4(b)	0	0	0.5
	O1 4(c)	0.463(5)	0.25	−0.071(7)
	O2 8(d)	0.281(5)	0.056(3)	−0.271(6)

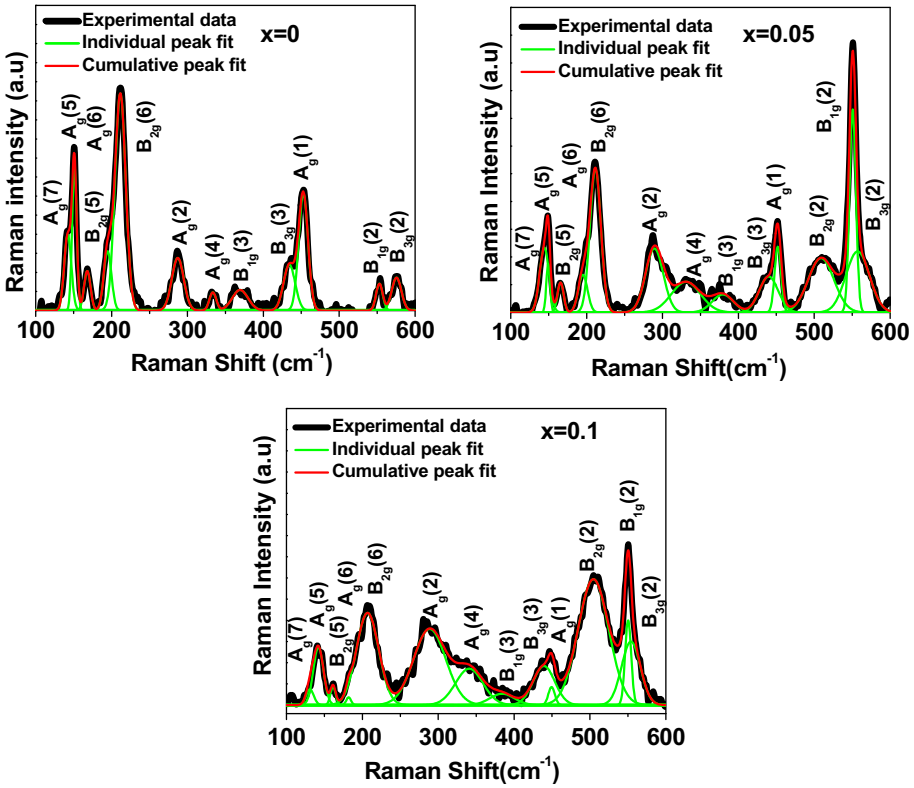

Figure 2. (colour online) Raman studies on $Nd_{1-x}Bi_xCrO_3$ ($x = 0$ and 0.1) compound at RT. The Raman modes are fitted with Gaussian profile method from 100 to 600 cm^{-1}.

Table 2. Raman modes at room temperature for $Nd_{1-x}Bi_xCrO_3$.

Assignment of modes	$x = 0$	$x = 0.05$	$x = 0.1$	Activating distortion	Atomic motions
$A_g(7)$	142	143	140	A-shift	
$A_g(5)$	151	149	142	rot[010]	A(x)
$A_g(6)$	195	195	181	rot[101]	CrO_6 in phase y rotations
$B_{3g}(5)$	168	165	161	rot[101]	
$B_{2g}(6)$	211	211	206	A-shift	A(Z), O1(Z)
$A_g(2)$	288	288	286	rot[010]	O1(x), A(–x)
$A_g(4)$	332	331	330	rot[101]	A(Z), O1(–Z)
$B_{1g}(3)$	367	379	386	rot[101]	CrO_6 out of phase x rotations
$B_{3g}(3)$	434	438	439	rot[101]	Out of phase O2 scissors like
$A_g(1)$	452	452	449	rot[010]	CrO_6 bendings
$B_{2g}(2)$	—	513	504	rot[010]	
$B_{1g}(2)$	551	551	550	rot[101]	CrO_6 out of phase bendings
$B_{3g}(2)$	575	569	554	rot[101]	O2, O1 anti-stretching

structural distortions, such as CrO_6 rotations has its impact on physical properties.

3.2 *Phonon studies*

Raman spectroscopy is a versatile technique to investigate the lattice dynamics of pervoskites and also reveal the local structural distortions due to CrO_6 rotations or displacement of cations in a unit cell. The irreducible representation of the Raman modes [33] for the orthorhombic pervoskite structure at the centre of the brillioun zone is given by equation (1).

$$\Gamma = 7A_g + 5B_{1g} + 7B_{2g} + 5B_{3g}. \quad (1)$$

Equation (1) shows the 24 Raman active modes possible for *Pnma* symmetry. Structural distortions in pervoskites are

generally attributed to atomic phenomena, which include rotation of CrO_6 octahedra, displacement of cations and Jahn–Teller (JT) distortion [34]. In the present study, the structural distortions are expected to happen either by the rotation of CrO_6 octahedra and/or A-site displacement of cations, whereas inactive JT ion (Cr^{3+}) cannot create any distortions within the unit cell. It is known that change in bond angles, bond lengths and tilt angles of the CrO_6 octahedra are decisive of functional properties of chromites [21,24]. The Raman spectra of NBiCO captured at RT is shown in figure 2 and the Raman mode assignments (shown in table 2) were performed in accordance to orthochromites [33–35]. To identify the Raman shift peaks for different 'Bi' substituted samples, the NBiCO Raman spectra were fitted in the range of $100-600\,cm^{-1}$ by a Gaussian profile [29] and each of the profile is characterized by three parameters, namely, frequency shift, intensity and line width. We observed 14 Raman modes out of 24 possible modes for *Pnma* structure. As we increase the substitution noticeable change in the phonon modes, like $A_g(5)$, $B_{3g}(5)$, $A_g(6)$, $B_{2g}(6)$ and $B_{3g}(2)$ shift to red frequency regime. The peak position depends on the natural vibrational frequency of the isolated molecule and the interactions with the environment. It is known that heavier atoms occupying at the A-site vibrates at low frequencies and that of light atoms like oxygen vibrate at relatively higher frequencies based on the relation $v\alpha(K/\mu)^{1/2}$, where K force constant depends on the interaction strength between atoms, v the frequency and μ the reduced mass [14]. Due to similar ionic radius of bismuth, the relative shift to red frequency is observed in the Raman modes like $A_g(6)$, $A_g(5)$, $B_{3g}(5)$ could be due to the heavier ion of Bi in Nd-site. The relatively heavier Bi cation could potentially alter the interactions among Nd–O modes and eventually, resulting in observed shift of $B_{2g}(6)$ ($5\,cm^{-1}$) and $B_{3g}(2)$ ($21\,cm^{-1}$) with 'Bi' composition and such significant changes observed in these phonon modes could be due to the weakening of interactions among A/B-site cation with oxygen atom and/or oxygen stretching modes. Thus, the Nd–O bond lengths observed from the XRD measurements are minor, but its effect is dominantly visible in our Raman studies. The octahedral rotations of CrO_6 as observed in $B_{1g}(3)$ and $B_{3g}(3)$, which shifts in blue frequency regime; i.e., increases the strength of interaction with bismuth composition. Thus, Bi substitution can create the short range forces, which lead to increasing the force constant and vibrational frequencies, become more effective with composition [36]. The interaction strength can only be observed when the bond distances/lengths are becoming closer with substitution. This can be seen from the minor decrease of Cr–O2 bond lengths and change in bond angles along Cr-O_2−Cr. The three modes $A_g(2)$, $A_g(4)$ and $B_{1g}(3)$ are observed as individual modes in NCO, whereas with substitution of Bi, they merge to a single broader phonon

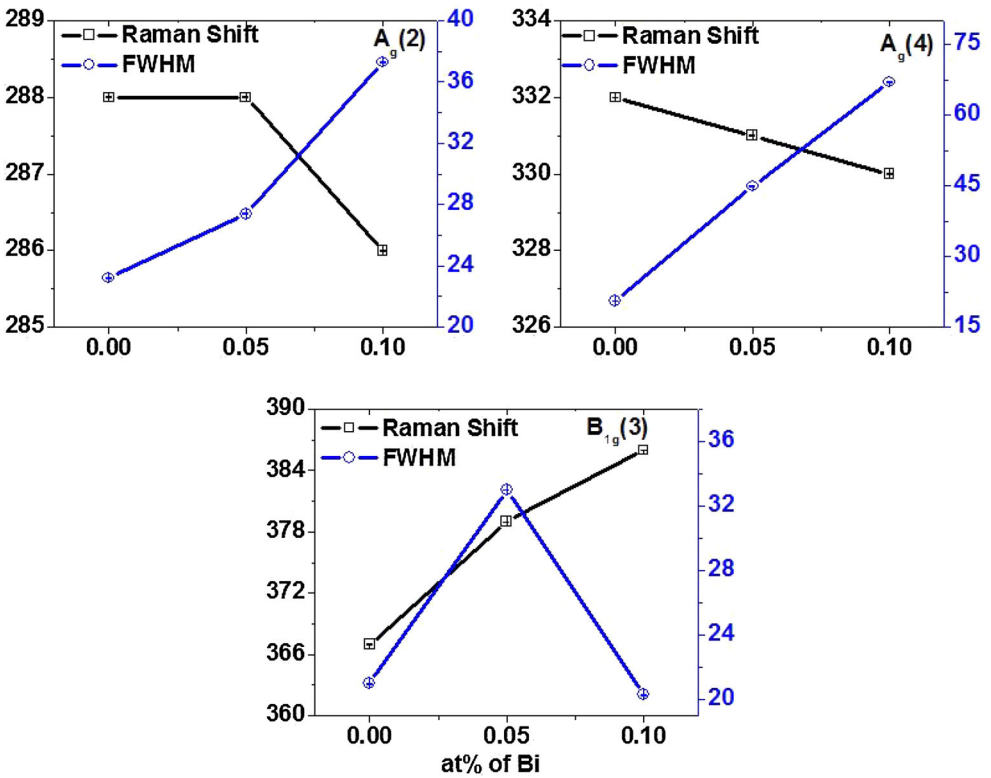

Figure 3. (colour online) Raman shift and FWHM variation of Ag (2), Ag (4) and B1g (3) with composition.

mode. The broader phonon mode was deconvoluted into three modes (∼280−370 cm^{-1}) and shown in figure 2 resulting from atomic motions related to A-cation and CrO_6 out of phase x-rotations. The variation of line widths (full-width half-maximum, FWHM) of three modes is shown in figure 3 and it shows that the FWHM are related to the environmentally induced frequency fluctuations due to electrostatic forces or inherent disorder leads to increase of broadening with bismuth [36,37]. In addition, we observe a unique Raman mode at $B_{2g}(2)$ (octahedral tilt, refer table 2) with an enhanced Raman intensity as composition increases, which might arise from the oxygen sublattice. The increased intensity of $B_{2g}(2)$ with composition reveals that the structural distortions introduced in NCO could be due to oxygen stretching modes at higher wavenumbers. The major changes observed with bismuth substitution in Raman modes suggest that the change in rotational and/or CrO_6 bending, Nd-displacement and oxygen stretching could collectively create the distortions observed. The structural distortions could arise from the octahedral site rotations plausibly arising from changes in the Cr–O and Nd–O bonds. However, these structural distortions on an average scale i.e., from XRD measurements are minor and the effects could be dominantly seen in Raman scattering experiments.

3.3 *Magnetic properties*

The magnetic molar susceptibility (χ_m) as a function of temperature (T) from 5 to 300 K in magnetic field of 100 Oe is plotted for zero field cooling (ZFC) and field cooled (FC) conditions (figure 4a). With the decrease in temperature, the first magnetic ordering (Neel transition temperature, T_N was obtained by using the derivative plots of magnetization as seen from the inset of figure 4b) was observed at 230 K for NCO, which is attributed to cooperative Cr^{3+} spin ordering. It is found that T_N decreases linearly from 230 ($x = 0$) to 223 K ($x = 0.1$). The Cr sublattice undergoes a long-range cooperative ordering transition that can be observed in drop of magnetization (around Neel transition) in $\chi_m - T$ measurements in NBiCO samples. Below T_N, the spontaneous magnetization first increases with decreasing temperature, reaching a maximum around $T = 187$ K. It then decreases and exhibits a minimum around $T = 100$ K, below which it again increases to a maximum at 35 K ($x = 0$). The unusual temperature dependence of magnetic behaviour can be explained by strong effective field on the Nd^{3+} moments by the ordered Cr^{3+} spin system [11]. Thus, below T_N, the Cr sublattice magnetization induces an effective magnetic field on Nd sublattice due to Nd–Cr interaction which tends to polarize the system from $\Gamma_2(F_x, Cy, Gz)$ into $\Gamma_1(A_x, Gy, Cz)$ at lower temperature (related to spin reorientation; $T_{SRPT} = 35$ K for $x = 0$) [26,38]. From figure 4a ZFC curves, we observed a small hump at $T \sim 10$–11 K, in all the samples from $x = 0$–0.1, whereas this hump is not observed in FC condition. The specific heat measurements on NCO system revealed that the hump at 10 K is due to the two-level Schtokky effect caused

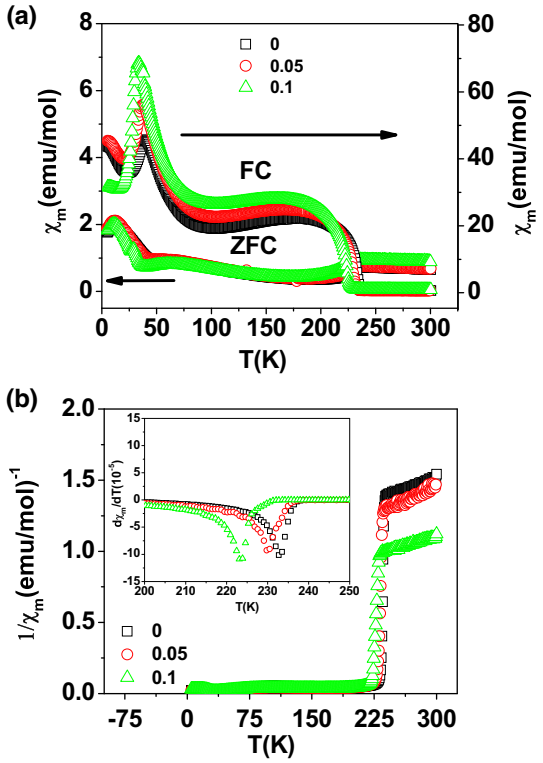

Figure 4. (colour online) The magnetic studies on $Nd_{1-x}Bi_xCrO_3$: (**a**) ZFC and FC done under the application of 100 Oe magnetic field and (**b**) inverse susceptibility with temperature (inset shows Neel transition temperatures obtained from the derivative plots).

by the split of 'Nd' ground doublet [38]. Doping Bi^{3+} into NCO, increases the magnitude of χ_m below transition temperature and has a strong effect on $\chi_m - T$ behaviour below the magnetic ordering temperature. The presence of nonmagnetic Bi^{3+} in magnetic site, Nd^{3+} site decreases the strength of interactions among the $Nd^{3+}-Cr^{3+}$ leads to decrease of T_{SRPT} from 35 ($x = 0$) to 28 K ($x = 0.1$). To elucidate the nature of the magnetic interaction above the transition temperature T_N, inverse susceptibility was plotted with T (figure 4b) following Curie–Weiss behaviour:

$$\chi^{-1} = \frac{3k_B\,(T - \theta_{CW})}{N_A \mu_{eff}^2}.$$

The Curie–Weiss fit was done at paramagnetic region of our samples and is shown in figure 5 for different compositions. The observed increase of effective magnetic moment values from Curie fit are 5.39 u_B ($x = 0$) − 6.72 u_B ($x = 0.1$), which is greater than the theoretical calculated values of 5.29 u_B for NCO ($\mu_{eff} = (\mu^2_{Nd3+} + \mu^2_{Cr3+})^{1/2}$, where $\mu_{Nd3+} = 3.62\,u_B$ and $\mu_{Cr3+} = 3.87\,u_B$). The observed higher values of effective magnetic moment is due to Curie–Weiss fitting done above 250 K, which is immediately above the transition temperature. The higher temperature fitting i.e., 2–3 times of transition

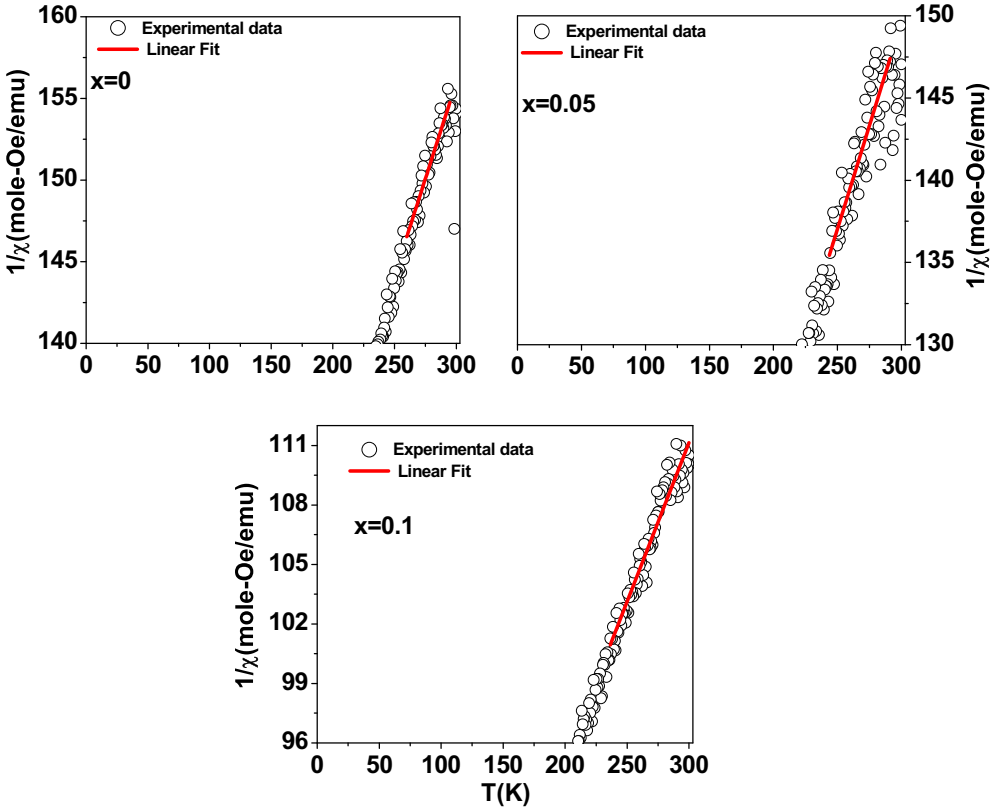

Figure 5. Curie–Weiss fitting from inverse susceptibility with temperature for different compositions.

Table 3. Coercive fields, Weiss temperature and Neel transition temperatures for different compositions.

	$x = 0$	$x = 0.05$	$x = 0.1$
$\boldsymbol{H}_c$ (Oe) at 5 K	184	450	445
$\boldsymbol{H}_c$ (Oe) at 100 K	40	175	823
Neel temperature (K)	230	228	223
Weiss temperature (K)	−389	−350	−345

temperature may give effective moment close to Cr^{3+} values. Table 3 shows the observed Weiss temperature (θ_{CW}), decreasing from −389 to −345 K. These values signify that increase of Bi concentration strengthens the ferromagnetic interaction or weakens the antiferromagnetic interactions. Figure 6a and b shows isothermal *M–H* loops at 5 and 100K for NBiCO, which shows that magnetization does not saturate up to 5 T. The coericivity varies from 184 ($x = 0$) to 445 Oe ($x = 0.1$) shown in figure 6a for $T = 5$ K ($T < T_{SRPT}$) (inset shows clear variation of *M–H* loops for $x = 0$ and 0.1) and the coericivity varies from 40 ($x = 0$) to 823 Oe ($x = 0.1$) at $T = 100$ K ($T_{SRPT} < T < T_N$) shown in figure 6b (inset shows clear variation of $M-H$ loops for $x = 0$ and 0.1). The room temperature *M–H* loops (not shown here) are almost straight lines indicating absence of any ferromagnetic ordering above Neel transition temperature.

It is worth remembering that the structural distortions due to Bi substitution in NCO lattice was evident from the structural studies such as change in phonon behaviour related to CrO_6 rotations as discussed in Raman can possibly facilitate this hybridization in NBiCO samples. Chromites with Cr^{3+} configuration, only π bonds of t^3-O-t^3 are present and eventually lead to an antiferromagnetic ordering. However, in $NdCrO_3$ structures, introducing plausible $t-e$ hybridization is expected to induce an additional structural distortion in the lattice associated with a change (reduction) in the antiferromagnetic interaction. Presence of such distortion facilitates virtual charge transfer (VCT) to the empty e component of the hybridized orbital, i.e., t^3-O-e^0, which effectively leads to observed weak ferromagnetic coupling [21] in our compounds. Thus, the present study Bi with similar ionic radii, but with a $6s^2$ lone pair configuration plausibly create the local structural distortions due to rotations of CrO_6 further leads to $t-e$ hybridization, which in turn changes the values of T_N in our chromites. The observed increase of 40–830 Oe above T_{SRPT} and 184 ($x = 0$) to 445 Oe ($x = 0.1$) below T_{SRPT} gives a clear indication that Bi^{3+} can influence greater in $Cr^{3+}-Cr^{3+}$ interaction than that of $Nd^{3+}-Cr^{3+}$ interaction. Thus, nonmagnetic Bi^{3+} alter the magnetic interactions of Nd^{3+} and Cr^{+3} ion coupling, which can be observed as a change in T_{SRPT} ($\Delta T \sim 7$ K with composition).

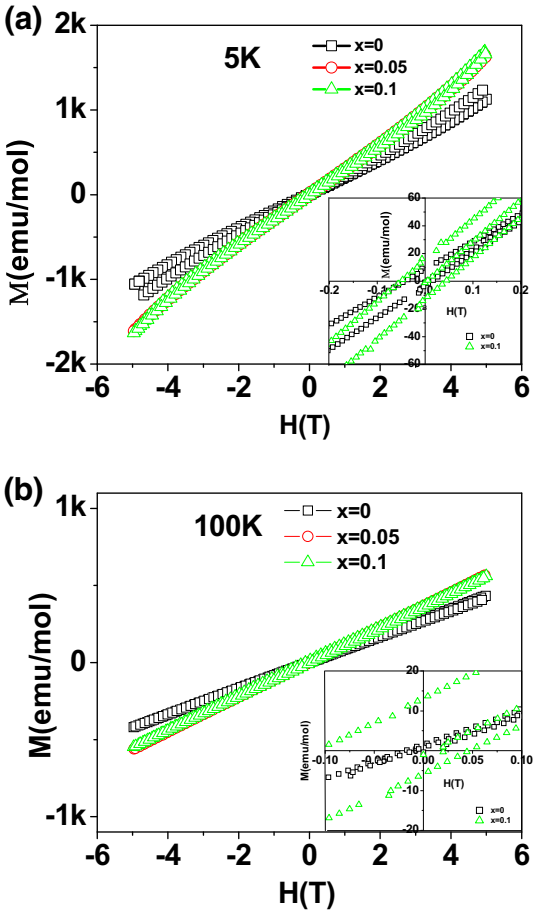

Figure 6. (colour online) Isothermal $M-H$ plots up to 5 Tesla at (**a**) 5 K and (**b**) 100 K for different compositions of bismuth. Inset shows zoom portion of $M-H$ loops for $x = 0$ and 0.1 at 5 and 100 K, respectively.

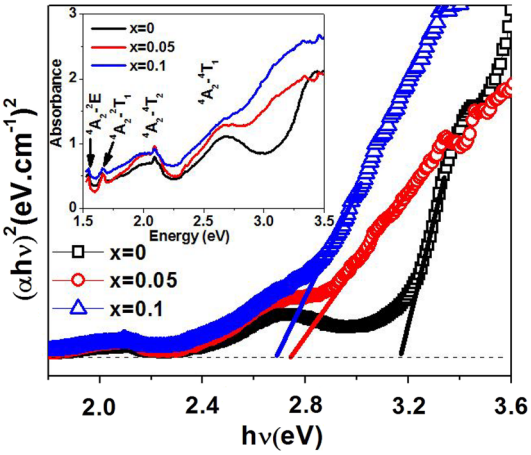

Figure 7. UV studies for calculation of bandgap NBiCO ($x = 0$ and 0.1). Inset shows optical absorption bands related to *dd* transitions.

3.4 *Optical studies*

Bi^{3+} cation is expected to interact strongly with the Cr–oxygen interaction and hence, the optical absorption features of NCO would be strongly influenced by Bi substitution. Hence, the optical absorption studies were carried out to study the influence on optical bandgap of NCO with Bi substitution. The optical absorption edge was analysed by the following relationship

$$\alpha h\upsilon = A\left(h\upsilon - E_g\right)^m,$$

where A is constant, m value is 1/2 and 2 for direct and indirect transitions, respectively, and E_g is the optical bandgap [39]. The optical absorption spectrum of Cr^{3+} ion in NBiCO was recorded at RT from $\lambda = 200-900$ nm. The absorption spectrum of NBiCO is typical of Cr^{3+} in a predominantly octahedral environment. The value of optical bandgap was estimated from the linear fitting and extrapolation of the $(\alpha h\upsilon)^2$ *vs*. $h\upsilon$ graph to the $h\upsilon$ axis bandgap of the compounds as shown in figure 7 and inset shows the absorption spectrum plotted with wavenumber. The studies reveal that the NCO ceramics have a direct bandgap characteristics and the absorption edge is observed at 3.1 eV for NCO. The absorption edge of NCO is primarily associated with the manifold of charge transfer transitions between O (2p) and Cr (3d) states [40] and this value decreases from 3.1 to 2.6 eV with increase of Bi content in NCO. The other optical absorption bands commonly observed in orthochromites arising from $d-d$ transitions of Cr^{3+} were also present. The optical absorption from ground state (electronic configuration of Cr^{3+} ion) $^4A_2-{}^4T_2$ and $^4T_1$ leads to observed two intense and broad bands were recorded at 16863 and 21645 cm^{-1}. In addition to that, two sharp bands at lower energies due to optical absorption from $^4A_2-{}^2T_1$ and ^2E_g at 13377 and 12446 cm^{-1} for NCO was also observed. The variation of optical absorption edge evidently suggests that Bi $(6s^2)$ substituted in the magnetic rare-earth Nd^{3+} influences the Cr–O overlap integral. This increase of interaction of Bi cation with oxygen bonds influences the structural distortions through Cr–O polyhedra [41]. Thus, the changes in rotational octahedra distortions observed through Raman scattering measurements and Cr–O changes through optical studies are in good agreement and this distortions that could plausibly be responsible for the observed changes in Neel transition temperatures as well as ferromagnetic nature in these compounds. Hence, the tunable optical properties such as bandgap from 3.1 to 2.6 eV and enhanced weak ferromagnetism (40 to 830 Oe) associated with structural distortions in NBiCO could be used for photocatalytic and magnetic applications [42,43].

4. Conclusions

$Nd_{1-x}Bi_xCrO_3$ ceramics with 'x' varying from 0 to 0.1 at% were successfully synthesized through sol–gel method. All

the compositions studied are stabilized in an orthorhombic *Pnma* structure, which was evident from the refinement studies. The variation of optical absorption edge evidently suggests that Bi ($6s^2$) substituted in the magnetic rare-earth Nd^{3+} influences the Cr–O overlap integral. This increase in interaction of Bi cation with oxygen bonds influences the structural distortions through Cr–O polyhedra were evident from the Raman studies. Nonmagnetic and similar ionic radius of Bi^{3+} in Nd^{3+} creates local structural distortions due to plausible nature of $6s^2$ electron configuration of Bi^{+3}. These structural distortions further influence the magnetic properties in our present study samples. The involvement of $t-e$ hybridization along with canting angle of Cr–O–Cr leads to the observed change in T_N from 230 to 223 K and T_{SRPT} from 35 to 28 K with Bi^{3+} content. Isothermal magnetization curves performed at 100 K ($T > T_{SRPT}$) shows increase of coercive field from 40 to 830 Oe and gives clear evidence of Bi^{3+} that can influence $Cr^{3+}-Cr^{3+}$ exchange interactions.

Acknowledgements

VRM and RR would like to acknowledge DST, India, and no. SERB/F/5142/2013-14/ for financial support to carry out the research.

References

[1] Sfeir J 2003 *J. Power Sources* **118** 276
[2] Minh N Q 1993 *J. Am. Ceram. Soc.* **76** 563
[3] Ngueteu Kamlo A, Bernard J, Lelievre C and Houivet D 2011 *J. Eur. Ceram. Soc.* **31** 1457
[4] Rajeswaran B, Khomskii D I, Zvezdin A K, Rao C N R and Sundaresan A 2012 *Phys. Rev. B* **86** 214409 (1–5)
[5] El Amrani M, Zaghrioui M, Ta Phuoc V, Gervais F and Massa N E 2014 *J. Magn. Magn. Mater*. **361** 1
[6] Serrao C R, Kundu A K, Krupanidhi S B, Waghmore U V and Rao C N R 2005 *Phys. Rev. B* **72** 220101(R) (1–4)
[7] Seo J-D and Son J Y 2013 *J. Cryst. Growth* **375** 53
[8] Ramesha K, Llobet A, Proffen Th, Serrao C R and Rao C N R 2007 *J. Phys. Condens. Matter* **19** 102202 (1–8)
[9] Sharma Y, Sahoo S, Perez W, Mukherjee S, Gupta R, Garg A *et al* 2014 *J. Appl. Phys*. **115** 183907 (1–9)
[10] Ray N and Waghmare U V 2008 *Phys. Rev. B* **77** 134112 (1–10)
[11] Hornreich R M 1978 *J. Magn. Magn. Mater.* **7** 280
[12] Shamir N, Shaked H and Shtrikman S 1981 *Phys. Rev. B* **24** 6642
[13] Sardar K, Lees M R, Kashtiban R J, Sloan J and Walton R I 2011 *Chem. Mater*. **23** 48
[14] Daniels L M, Weber M C, Lees M R, Guennou M, Kashtiban R J, Sloan J, Kreisel J *et al* 2013 *Inorg. Chem.* **52** 12161
[15] Yoshii K 2012 *Mater. Res. Bull*. **47** 3243
[16] Su Y, Zhang J, Li L, Li B, Zhou Y, Deng D *et al* 2010 *Appl. Phys. A***100** 73
[17] Artem'ev G G, Kadomtseva A M, Milov V N, Lukina M M and Mukhin A A 1995 *J. Magn. Magn. Mater.* **140–144** 2157
[18] Horneriech R M, Komet Y and Wanklyn B M 1972 *Solid State Commun*. **11** 969
[19] Su Y, Zhang J, Feng Z, Li L, Li B, Zhou Y *et al* 2010 *J. Appl. Phys.***108** 013905 (1–6)
[20] Cooke A H, Martin D M and Wells M R 1974 *J. Phys. C: Solid State Phys*. **7** 3133
[21] Treves D, Eibschutz M and Coppens P 1965 *Phys. Lett*. **18** 216
[22] Zhou J S, Alonso J A, Pomjakushin V, Goodenough J B, Ren Y, Yan J Q *et al* 2010 *Phys. Rev. B* **81** 214115 (1–5)
[23] Dunitz J D and Orgel L E 1957 *J. Phys. Chem. Solids* **3** 20
[24] Wang S, Huang K, Hou C, Yuan L, Wu X and Lu D 2015 *Dalton Trans*. **44** 17201
[25] Zhou J S and Goodenough J B 2006 *PRL* **96** 247202 (1–4) and 2008 *Phys. Rev. B* **77** 132104 (1–4)
[26] Lufaso M W, Mugavero S J, Gemmill W R, Lee Y, Vogt T and Zur Loye H-C 2007 *J. Alloys Compd*. **433** 91
[27] Hornreich R M, Komet Y, Nolan Y R, Wanklyn B M and Yaeger I 1975 *Phys. Rev. B* **12** 5094
[28] Chakraborty K R, Mukherjee S, Kaushik S D, Rayaprol S, Prajapat C L, Singh M R *et al* 2014 *J. Magn. Magn. Mater.* **361** 81
[29] Satoh H, Koseki S, Takagi M, Chung W Y and Kamegashira N 1997 *J. Alloys Compd*. **259** 176
[30] Du Y, Cheng Z X, Wang X-L and Dou S X 2010 *J. Appl. Phys*. **108** 093914 (1–9)
[31] Neaton J B, Ederer C, Waghmare U V, Spaldin N A and Rabe K M 2005 *Phys. Rev. B* **71** 014113 (1–8)
[32] Niitaka S, Azuma M, Takano M, Nishibori E, Takata M and Sakata M 2004 *Solid State Ionics***172** 557
[33] Rodrigues-Carvajal J 2000 *An introduction to the program fullprof Rietveld refinement and pattern matching analysis* (France: Laboratoire Leon Brillioun CEA-CNRS)
[34] Abrashev M V, Bäckström J, Börjesson L, Popov V N, Chakalov R A, Kolev N *et al* 2002 *Phys. Rev. B* **65** 184301 (1–9)
[35] Weber M C, Kreisel J, Thomas P A, Newton M, Sardar K and Walton R I 2012 *Phys. Rev. B* **85** 054303 (1–9)
[36] Todorov N D, Abrashev M V, Ivanov V G, Tsutsumanova G G, Marinova V, Wang Y-Q *et al* 2011 *Phys. Rev. B* **83** 224303 (1–6)
[37] Schindler W and Jonas J 1980 *J. Chem. Phys*. **72** 5019
[38] Schweizer K S and Chandler D 1982 *J. Chem. Phys*. **76** 2296
[39] Bartolomé F, Bartolome J, Castro M and Melero J J 2000 *Phys. Rev. B* **62** 1058
[40] Gu F, Wang S F, Lu M K, Zhou G J, Xu D and Yuan D R 2004 *J. Phys. Chem. B* **108** 8119
[41] Zenkov A V 2008 *Res. Lett. Phys.* (https://doi.org/10.1155/2008/749305)
[42] Tripathi A K and Lal H B 1980 *Mater. Res. Bull.***15** 233
[43] Shukla R, Manjanna J, Bera A K, Yusuf S M and Tyagi A K 2009 *Inorg. Chem.* **48** 11692
[44] Shukla R, Bera A K, Yusuf S M, Deshpande S K, Tyagi A K, Hermes W *et al* 2009 *J. Phys. Chem. C***113** 12663